ACS OMEGA

http://pubs.acs.org/journal/acsodf

Article

Limit-Defying μ-Total Analysis System: Achieving Part-Per-Quadrillion Sensitivity on a Hierarchical Optofluidic SERS Sensor

Subhavna Juneja,[§] Boxin Zhang,[§] and Alan X. Wang*

Cite This: *ACS Omega* 2023, 8, 17151−17158

Read Online

ACCESS | Metrics & More | Article Recommendations | Supporting Information

ABSTRACT: Optofluidic sensors have accelerated the growth of smart sensor platforms with improved sensitivity, reliability, and innovation. In this article, we report the integration of a surface-enhanced Raman scattering (SERS) material consisting of silver nanoparticle-decorated diatomaceous earth (AgNPs−DE) with a flow-through microfluidic device, building up a hierarchical structured micro-total analysis system (μ-TAS) capable of achieving part-per-quadrillion (ppq)-level sensitivity. By the synergic integration of millimeter-scale microfluidic devices and porous laboratory filter paper with a micrometer-sized crosslinked cellulosic network that carries SERS-active AgNPs−DE, which possesses submicron to nanometer regimes of photonic crystals and plasmonic nanostructures, we achieved enhanced mass-transfer efficiency and unprecedented detection sensitivity. In our experiment, fentanyl as the testing analyte at different concentrations was measured using a portable Raman spectrometer. The limit of detection (LOD) was estimated to be 10 ppq from a small detection volume of 10 mL with an ultrafast time of sensing (TOS) of 3 min. To attain comparable signals, the traditional soaking method took more than 90 min to detect 10 part-per-trillion fentanyl from a 10 mL sample. Compared with existing SERS sensing results of fentanyl, the limit-defying μ-TAS reduced the LOD-TOS product by almost 4 orders of magnitude, which represents a new stage of ultrafast sensing of extremely low concentration analytes.

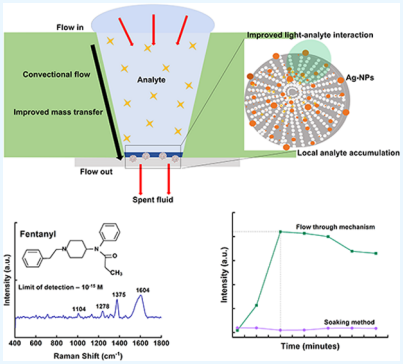

1. INTRODUCTION

Device miniaturization and sensor fusion have been consistent driving forces toward the ingenuity, progress. and sustainability of intelligent sensing platforms.[1−3] The surging interest in small devices arises from their versatility, broad-spectrum applicability, screening precision, device mobility, multiplexing ability, speed, and reduced analyte requirement.[4−7] Following the development of the first ever miniature device, the gas chromatographic air analyzer,[8] to the present day micro-total analysis system, micro-/nanofabrication has greatly influenced the research efforts and commercial product viability globally.[9−12] The ease of manipulating fluids in microchannels, laminar-flow-driven controlled movement, smaller diffusion time, and thereby a higher signal-to-noise ratio predominantly explain the higher sensitivity in reduced-scale devices.[13] Sensors with photonic characteristics such as surface-enhanced Raman scattering (SERS)-based sensing, both biological and chemical, are no exception and are often integrated with microfluidic functions to achieve improved practical sensing platforms. SERS-assisted sensing is found to be specific, label-free, having sensitivity comparable to fluorescent techniques, yet maintaining simpler optical system requirements and higher multiplexing density.[14] Different approaches, for instance, in situ nanoparticle growth, nanostructure aggregation in microchannels, or on-chip analyte−nanoparticle mixing, have been previously explored as possible pathways to improve the sensing efficiency of optofluidic SERS devices.[15−18] However, ultrasensitive detection limits up to the femtomolar level or beyond are yet to be achieved. In addition to the adsorption−desorption characteristics and diffusion kinetics of the analyte, which dictate the accumulation efficiency in the detection volume, in small devices, the analyte flux at any time is much lower than that in conventional diffusion methods such as drop-casting or diffusion-assisted soaking.[19] While microfluidic automation adds to the precision and control in sample processing, limiting the analyte flux compromises the sensing efficiency.

A viable proposition to develop a sensing platform with the advantages of both the constituting components, microfluidic and photonic, is to tailor altered analyte mass transportation routes and improved light−analyte interaction in the detection volume.[19−21] Directed analyte accumulation through constricted device channels, where the analyte follows a convective pathway as opposed to diffusion (in planar substrates), improved the sensor performance by maintaining a significantly high analyte concentration, within the detection volume, at all times, for measurable signal generation.[22,23] As important as it is to retain a high molecular flux, it often requires

Received: March 6, 2023
Accepted: April 19, 2023
Published: May 1, 2023

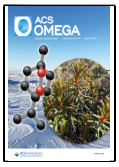

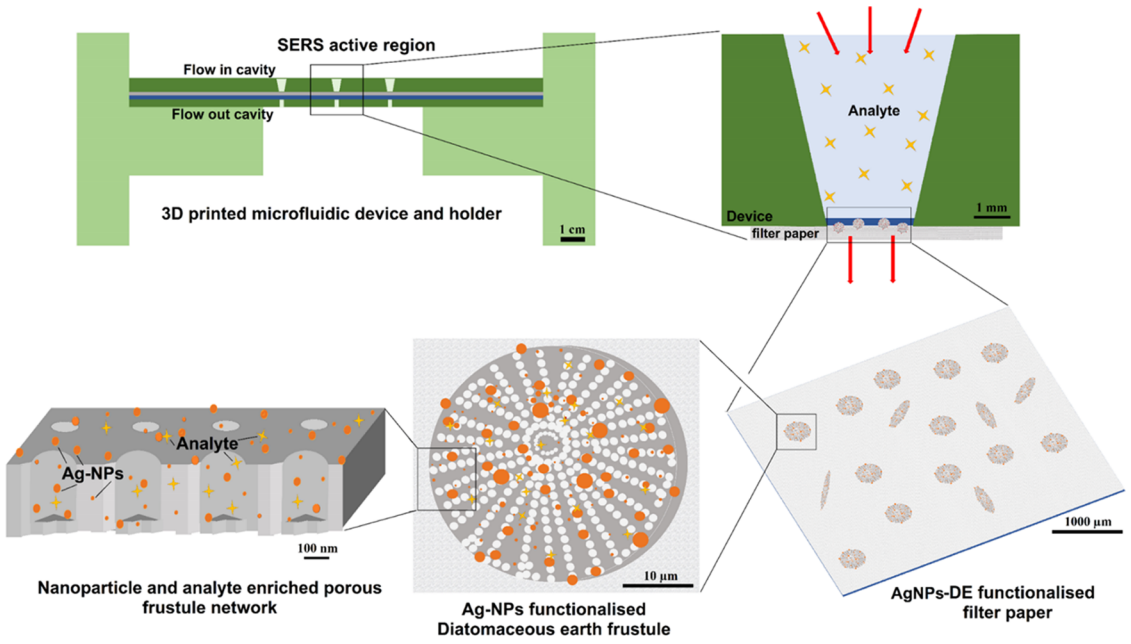

Figure 1. Schematic representation of the fabricated hierarchical optofluidic sensor. Different panels represent the various levels of the sensing platform assisting in improving the SERS signals, resulting from the altered mass-transfer pathway and increased light−analyte interaction.

enhancement complementation from nanoparticles to achieve extremely low detection limits.[24] An improved signal intensity within the detection volume channeled through nanostructures can be achieved by (a) expanding the detection volume, for example, accumulating signals along the entire photonic crystal fiber length or waveguide, or (b) using active or passive routes to improve analyte interaction. It includes using active forces such as conductive, magnetic, or electrokinetic forces or nanoparticle trapping within microfluidic channels to passively accumulate small molecules between the nanogaps[25−28] to increase the local analyte concentration and thus SERS signals. FRET-conjugated optofluidic ring resonators, nanohole arrays, and silver nanoparticle/graphene oxide-coated optofluidic capillaries are some recent examples from the literature emphasizing a drastic SERS performance improvement by limiting the dependence on diffusive pathways for fluid flow, molecular enrichment by following capillary action, and improved light−analyte interaction.[20,21] Optofluidic SERS devices are by far one of the most sophisticated screening platforms available conventionally. However, they are limited in throughput and sensitivity, mainly due to inefficient mass-transfer routes.[29]

In an effort to develop optofluidic systems capable of ultrasensitive screening, through this work, we present a SERS-based integrated hierarchal microfluidic device. Figure 1 schematically illustrates the device design and the different hierarchical levels constituting the optofluidic platform. The fabricated device utilizes the photonic and fluidic characteristics of the naturally occurring photonic crystals, diatomaceous earth, to capture, concentrate, and screen the analyte, replicating an operational μ-total analysis system (μTAS). The optofluidic-μTAS, at the first level, comprises the regularly used laboratory filter paper, carrying silver nanoparticle-functionalized diatomaceous earth (AgNPs−DE). The millimeter-scale filter paper plays a dual role, where it not only helps hold the functionalized AgNPs−DE within its cellulose network but also assists in fluid flow using capillary forces. In the second level of our sensing surface, the cellulose crosslinking network forming indigenous microcavities holds the functionalized diatomaceous frustules mimicking a high-density array of microfluidic channels. Finally, the submicron array of quasipores on the diatomaceous earth features form the third and final sieving layer of our device, helping in capturing the analyte molecules onto the sensor surface where plasmonic hotspots are present. The arrayed pores in the frustules are characterized by photonic crystal characteristics, which, when utilized in combination with plasmonic metal centers, as silver nanoparticles in our case, improve the SERS efficiency[20] by providing a larger light−analyte interaction surface area. To summarize, as the test fluid passes through the various levels in our device, the asymmetry in the size of the porous cavities drives the fluid to follow a convective rather than the conventional diffusive route. In addition, the surface properties and porous nature of the contributing device layers assists in increasing the contact surface by generating multiple analyte interaction sites and improving the mass-transfer properties, which, in synergy with the optical manipulation of light due to the Ag−DE composite, drives the working mechanism of the developed μ-TAS to achieve high sensitivity.[21]

The capability of our device to detect extremely low levels of analyte concentrations is an additive response to an ideal interplay of device design and the choice of sieving material and its associated properties. For instance, engineered through design, because of the differently sized pores in the various levels of our device, the fluid flow induced accelerated mass transfer. Convection flow establishes analyte movement from regions of high to low density, leading to translational local accumulation of the analyte in DE cavities.[19,21,30,31] This device-directed analyte accumulation is further improved or supported by the biochemical and porous nature of our choice of substrate material i.e., DE. Because of their biological origin, the DE surface is rich in anionic silanol groups that bestow them with hydrophilic characteristics, helping in drawing and retaining more test fluid in the cavities.[32−34] However, the porosity in DE increases the specific surface area by

https://doi.org/10.1021/acsomega.3c01519
ACS Omega 2023, 8, 17151−17158

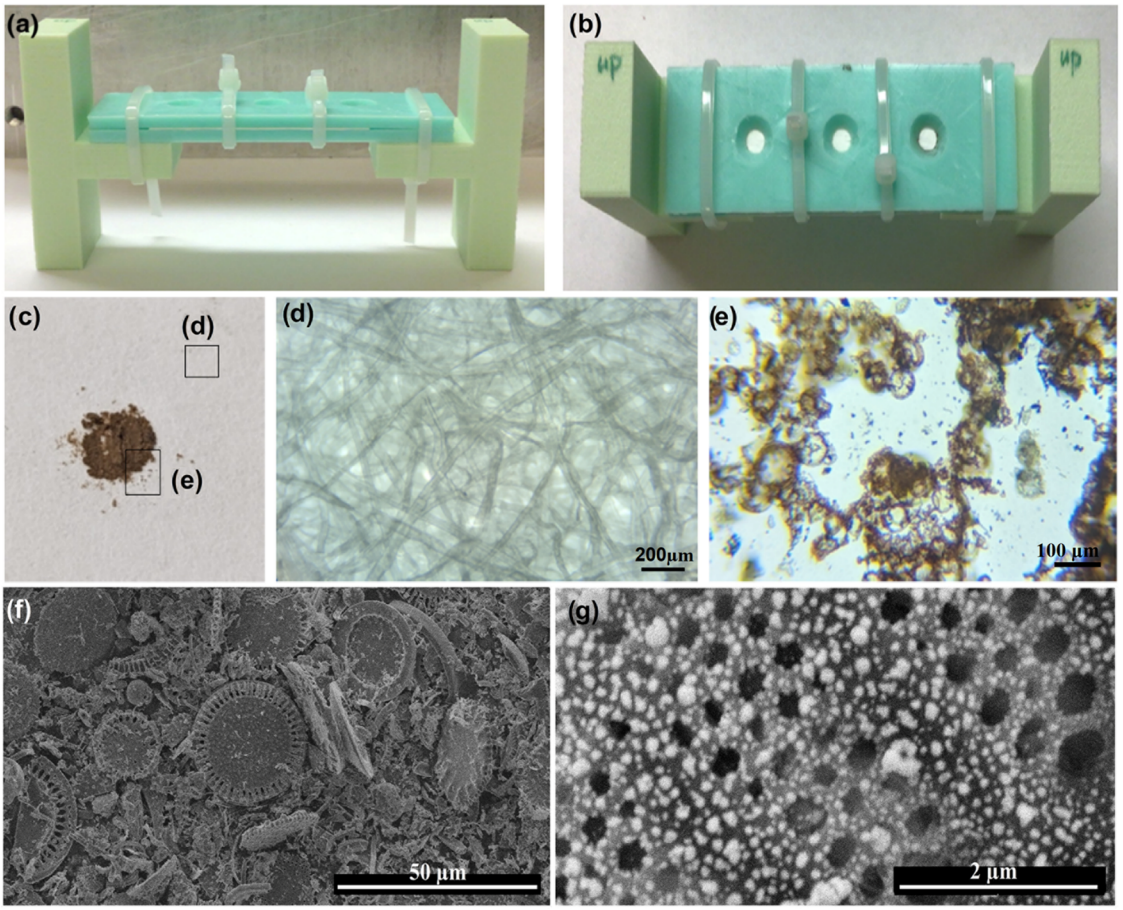

Figure 2. (a, b) Images of the side and top views of the fabricated microfluidic device and holder. (c) Image of the Ag−DE-functionalized paper substrate used for SERS screening. (d, e) Images of the Ag−DE-functionalized filter paper acquired from two selective regions representing the cellulose network and Ag−NP-functionalized DE, respectively. (f, g) Low- and high-magnification SEM images of the features of disk-shaped diatomaceous earth and silver nanoparticles lining the DE surface and pores.

introducing multiple interaction sites in the exposed cavity walls, contributing to a high analyte flux at any time.[35−37] The device-directed analyte accumulation is further complemented by the improved Raman scattering due to the silver-functionalized DE lining the final level of the sensing device. Compared to DE or silver nanoparticles alone, the optical potential of plasmonic-functionalized DE to tune Raman scattering is much superior. Ag−DE not only gains significant contribution from the electromagnetic characteristics of the functionalizing nanoparticles, leading to improved analyte−light interaction, but due to their well-defined structure, it also exhibits a high density of hotspots,[27,28,38,39] contributing to an improved signal-to-noise ratio. The choice of SERS for analyte screening is also aimed to achieve specificity and universal utility of the developed sensing platform.

For this study, the synthetic opioid, fentanyl, at different concentrations in spiked drinking water was tested for application in environmental monitoring. The limit of detection achieved was 10 part-per-quadrillion (ppq or 10^{-15}) while the measurement time was 3 min. The improvement in the sensing performance when compared with different fentanyl sensing platforms from the literature was estimated to be approximately $10^4\times$. Synergistic contributions of the devised sieving methodology, dimensional interplay through the different levels of the sensing device, and detection volume expansion are considered to be the major contributing factors to the high sensitivity achieved.

2. RESULTS AND DISCUSSION

2.1. Characterization of the SERS-Active AgNPs−DE Material. The SERS-active filter paper comprising of the AgNps−DE composite was supported between the layers of a 3D printed platform, as shown in Figure 2a,b. Before characterization of the active material by electron microscopy, a simple optical microscope was used to gain insights into the structural details of the different constituting components of the hierarchical device. Digital and optical images of a representative section on the SERS substrate comprising of the crosslinked cellulose network and skeletal features of diatomaceous earth in low magnification are shown in Figure 2c−e. The prepared SERS-active material shows the discrete presence of features of diatomaceous earth, exhibiting a disk-shaped morphology and a continuous network of porous structures lining their surface. As observed under a scanning electron microscope (SEM), the surface of the skeletal diatomaceous earth was also marked by the uniform presence of quasispherical silver nanoparticles. The nanoparticles were densely packed with a nearly monodisperse population. Representative SEM images are shown in Figure 2f,g. The average sizes of the functionalized Ag nanoparticles are found to be 52 ± 1.1 nm (Supporting Figure S1a). An aqueous

https://doi.org/10.1021/acsomega.3c01519
ACS Omega 2023, 8, 17151−17158

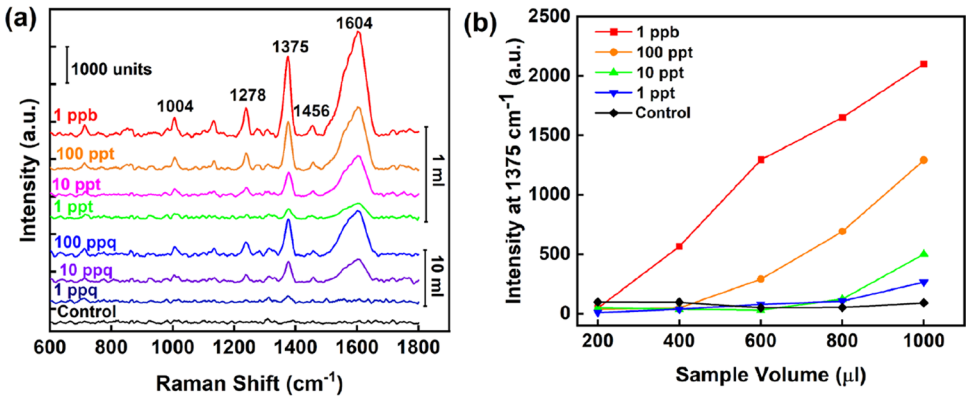

Figure 3. (a) SERS spectra of different concentrations of fentanyl molecules (1 ppb to 1 ppq) on SERS-active DE filter paper acquired by the flow-through method. The notations 1 and 10 mL represent the sample volumes used to acquire the SERS spectra for fentanyl concentrations above and below 1 ppt, respectively. (b) Graphical representation of the variation in the SERS intensity for different tested fentanyl concentrations as a function of the sample volume.

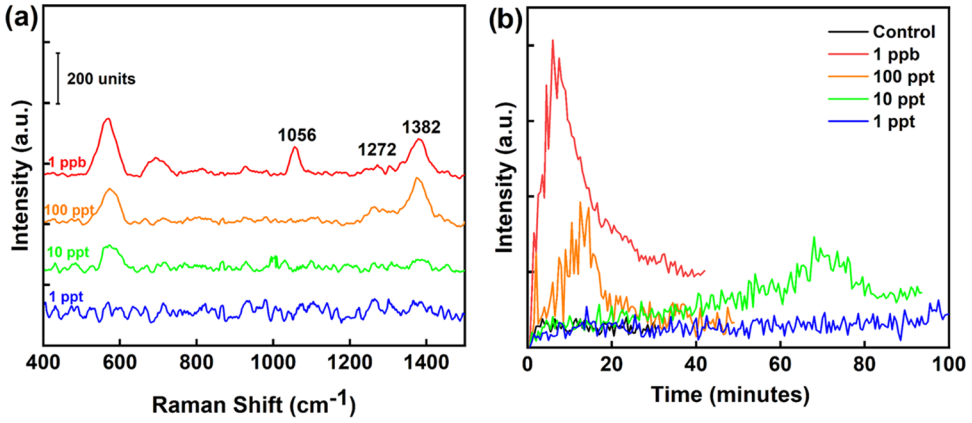

Figure 4. (a) SERS spectra of different fentanyl concentrations on SERS-active DE using the traditional soaking methodology. (b) Graphical representation of variations in the SERS signal for different concentrations of fentanyl as a function of the measurement time.

solution of the prepared powder was used to acquire UV−visible spectra to gain insights into its plasmonic behavior. SERS-active diatomaceous earth (DE) shows sensitivity to the visible light region, with a broad, clear absorption peak centered at 420 nm, characteristic of the localized surface plasmon resonance (LSPR) originating in nanostructured silver upon interaction with light.[40,41] No additional absorption features were observed, indicating sample purity. The obtained spectrum is presented in Figure S1b.

2.2. SERS Performance for Fentanyl Detection. *2.2.1. μ-TAS by Flow-Through Testing.* The μ-TAS was tested by a portable Raman spectrometer. A regular clinical syringe filled with the analyte, fentanyl, was positioned at the center of the flow-in cavity and attached to a peristaltic pump to control the fluid flow. At regular intervals of time, equal volumes (50 μL) of fentanyl solution were dispensed from the syringe onto the prepared substrate, followed by a Raman measurement. The process was repeated for all of the tested concentrations of fentanyl (1 ppb to 10 ppq). Characteristic fentanyl SERS spectra acquired on the fabricated SERS optofluidic device are shown in Figure 3a. Four major vibrational modes of fentanyl molecules appearing at 1004, 1278, 1375, and 1604 cm^{-1}, indexed to the C−C−C trigonal bend B1, C−H twisting C3, C−H bond C7, and C−C symmetric stretch of B1, respectively, were marked.[42,43] As the fentanyl concentration decreased from 1 ppb to 1 ppt, the vibrational reflections showed a proportional drop in signal intensity, indicating the direct correlation of the Raman signal intensity with the number of analyte molecules. In addition to the series of fentanyl concentrations measured, a volume-dependent study was also performed, where, for all four tested fentanyl concentrations, 1 ppb, 100 ppt, 10 ppt, and 1 ppt, different volumes ranging between 200 and 1000 μL were flown through the device to map the kinetic trend and estimate the lowest detection volume required to obtain measurable signals. The intensity trend of the SERS signal at one of the characteristic peaks, 1375 cm^{-1}, as a function of the sample volume, for the four tested fentanyl concentrations is displayed in Figure 3b. Increasing the sample volume, as expected, followed an upward direct trend, where a greater volume led to a higher signal because of the larger number of molecules residing in the detection volume. With the exception of the high concentration of 1 ppb, none of the other concentrations showed any significant signal generation for testing volumes <600 μL. Lower testing volumes resulted in compromised device sensitivity. Therefore, considering the statistical validation of the acquired data, a minimum sample volume of 1 mL was fixed to be an ideal working sample volume for efficient testing using the fabricated device model. Representative SERS spectra as a function of volume for all of the different fentanyl concentrations are presented in Figure S2a−d (Supporting Information).

https://doi.org/10.1021/acsomega.3c01519
ACS Omega 2023, 8, 17151−17158

To estimate the testing saturation and sample-carrying capacity, different volumes of fentanyl solution were flown through the device. Considering that the Raman intensity has a direct relationship with the analyte concentration, with increasing volume, more analyte molecules were available in the detection volume and thus a higher signal was attained (data not shown). At an increased testing volume of 10 mL, we observed that the device was capable of pushing the limit of detection by an order of 100 and was able to sense fentanyl concentrations even at 10 ppq. The representative SERS spectra are presented in Figure 3a. In the spectrum, we also see the Raman signal for a fentanyl concentration of 1 ppq. However, considering that the signal intensity was very faint and the estimated signal-to-noise ratio (SNR) was below 3, which is the minimal acceptable peak confidence level,[27] 1 ppq was not taken into consideration for tabulating the lowest detectable limit and 10 ppq was marked as the LOD for the adopted flow-through testing on μ-TAS.

2.2.2. SERS Sensing by the Traditional Soaking Method. To compare the performance of the traditional, diffusion-dominant soaking method with our hierarchal optofluidic device, a set of control experiments were performed. Replicating the usual soaking methodology, our fabricated SERS-active DE substrates were soaked into different concentrations of aqueous fentanyl solution, followed by Raman measurements (Figure 4a). The signal-to-noise ratio for the soaking method was observed to decrease significantly, with the presence of very feeble signal reflections mapped only at the parent position of 1375 cm^{-1} corresponding to the C−H twisting in C3. Vibrational signals at other characteristic wavenumbers were near negligible and comparable to the noise level. The LOD for the soaking methodology was marked as 10 ppt. The performance efficiencies of the two methods were tested against two parameters: (a) the measurement time and (b) the lowest detectable fentanyl concentration. The SERS intensity for fentanyl molecule vibration at 1375 cm^{-1} as a function of the testing time is depicted in Figure 4b. For concentrations ranging from 1 ppb to 10 ppt, the Raman signal intensities were observed to first increase and then decrease as a function of the measurement time. The threshold cutoff time, following which the downward signal intensity trend was observed, varied with fentanyl concentration. As a larger number of analyte molecules are available at higher concentrations, substrate saturation is achieved much faster, the signal intensity is higher, and the threshold time is smaller. For example, for 1 ppb, the highest signal intensity was obtained within 10 min; however, for 10 ppt, a saturation time of approximately 70 min was required. While the initial increase in the signal intensity is ascribed to time-dependent analyte saturation, the following drop in signal intensity beyond the threshold is often associated with emitted SERS photon reabsorption, resulting in signal quenching.[44]

For all of the tested fentanyl concentrations ranging from 1 ppb to 1 ppt, the measurement time was much higher when compared to optofluidic-based testing. As an example, a 1 ppb fentanyl solution required an average response time of 10 min to achieve a measurable signal on the planar substrate compared to the measurement time of less than 1 min on the optofluidic platform. In addition, the analyte requirement of 1 mL, optimized through the flow-through experiments, was found to be not enough to generate detectable SERS signals under the soaking method conditions. For soaking experiments, the minimum analyte volume required for testing was estimated as 10 mL (data not shown). It was also observed that, within the stipulated experimental testing time, fentanyl concentrations below 10 ppt, irrespective of the increased analyte volume at 10 mL, were not detectable on the SERS substrates by the traditional soaking procedure. The soaking method thus displayed poor performance in terms of both response time and LOD.

2.2.3. Comparison with State-of-the-Art SERS Sensing for Fentanyl. To emphasize the importance of our study, a performance comparison with similar high-throughput SERS-based devices, fabricated and tested for fentanyl screening, was performed.[45−52] A representative graph is presented in Figure 5. Compared to different testing methodologies, we found our

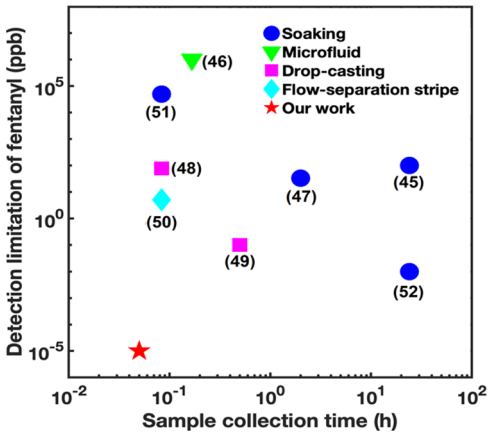

Figure 5. Comparison of the performance of the μTAS SERS optofluidic device fabricated by us with other similar devices in the literature.

device to exhibit a superior performance. In terms of LOD and measurement time, the device fabricated by us shows a performance increase by an order of 4 times.

3. CONCLUSIONS

In this work, we present a μTAS optofluidic screening platform engineered through design to achieve an extremely high sensitivity. A scale-directed modified fluid flow pattern, altered optical characteristics of the hybrid AgNPs−DE, and the sensitivity of SERS to spectroscopic screening, in synergism, contributed to achieving a limit of detection as low as 10 ppq. For our testing analyte, fentanyl, screened over different concentrations, the analyte volume and concentration were observed to have a direct relationship with the SERS intensity. In order to achieve detection at extremely low concentrations, the time of measurement was not compromised as all of the detection spectra were acquired within 3 min. The performance of the optofluidic platform was compared with the traditional soaking methodology. The limit of detection achieved on soaking substrates was only 10 ppt, while the testing time lasted several minutes to hours. Improved analyte accumulation, augmented light−analyte interaction, and a channelized flow-through pathway for fluid movement are ascribed to be key contributors to the achieved ultrasensitivity. The limit-defying μTAS optofluidic platform reduced the LOD-TOS product by almost 4 orders of magnitude, which represents a new stage of ultrafast sensing of extremely low concentration analytes. Although the developed device shows excellent testing capability, utilizes a very small sample volume,

https://doi.org/10.1021/acsomega.3c01519
ACS Omega 2023, 8, 17151−17158

shows improved mass-transfer properties, is precise, simple, and rapid, it certainly faces some challenges in terms of complex (biological fluid) or multifunctional sorting and detection, where precise fluid manipulation, sample sorting, and manufacturing complex 3D fluidic designs will be some key parameters to be addressed in the future.

4. EXPERIMENTAL DETAILS

4.1. Preparation of the SERS-Active Biophotonic Crystal. A simple two-step process comprising of (a) filtration and (b) in situ chemical reduction was adopted to fabricate the hybrid plasmonic−photonic crystal SERS substrates. The as-received diatomaceous earth (DE), Celite 209, was weighed and mixed with Milli-Q water to form an aqueous solution. As DE powder is prone to lumping, it was added in parts and mixed continuously to form a uniform solution. The final mix was sieved through a Whatman filter paper having a pore size of 30 μm to filter out any irregular, broken, or smaller skeletal features and achieve a nearly monodisperse frustule population. Following separation, the filtrate was collected and maintained in an oven overnight at 230 °C for drying and activation. For the in situ growth, a previously optimized protocol with slight modifications was used.[52−54] In brief, 3 g of the filtered diatomaceous earth (f-DE) was weighed and mixed in an aqueous nucleation solution containing a 1:1 (w:w) ratio of stannous chloride/HCl. The optimal reaction time to generate significant nucleation sites is 15 min. The charged f-DE was separated from the nucleation solution, washed thoroughly, and added to a fresh solution of 20 mM $AgNO_3$ to allow the formation of silver seeds at the nucleation loci. This reaction step was also maintained for 15 min. Next, f-DE was separated from the seed solution and added to an aqueous mixture of $AgNO_3$ (5 mM)/L-ascorbic acid (20 mM) growth solution, prepared in a working ratio of 8:1 (v:v). The functionalized DE powder was separated from the growth mix, washed thoroughly with Milli-Q water, and finally dried at room temperature to yield a SERS-active DE powder.

4.2. Design and Fabrication of the Substrate Platform. To achieve higher sensitivity and maintain continuous analyte pumping for the flow-through analysis, a 3D holder platform was printed using the 3D printing facility maintained at the Valley Library at the Oregon State University. The printed holding device consisted of four prominent subparts: a top lid or the flow-in plate, a bottom lid or the flow-out plate, and two side supports for holding the lids, as shown in Figure 2a,b. Three funnel-like depressions were carved out of each lid having top and bottom diameters of 4 and 2 mm, respectively. The titling angle between the top and bottom surfaces was maintained at 45° such that, while sample pumping, as a consequence of volume constriction, enough pressure to sieve the analyte through the cellulose network is created. As the sample is drawn from the surface into the diatom frustule pores through the capillary action, it results in local analyte accumulation, achieving detectable analyte concentration, even at trace levels.

4.3. Preparation of SERS Substrates. 500 mg of the SERS-active material was mixed with 1 ml of Milli-Q water to form the substrate coating mix. For each SERS-active substrate, 50 μL of this mix was drop-soaked onto a Whatman filter paper of dimension 5 × 5 mm^2 and allowed to air dry before placing on the platform for SERS measurement. Representative digital and microscopic images of the SERS-active substrates are presented as Figure 2c−e. Morphological and plasmonic characteristics of the silver nanoparticles on f-DE were studied by scanning electron microscopy (SEM) and UV−visible spectroscopy, respectively.

4.4. Raman Measurement and Data Processing. The synthetic opioid, fentanyl, was used as a model drug to test the screening efficiency of the fabricated SERS substrates and the proposed methodology. Using serial dilution, a series of working solutions of fentanyl (10^{-9}−10^{-15} M) were prepared in Milli-Q water. Before spectral recording, for the flow-through analysis, corresponding to each testing concentration, 50 μL of the solution was sieved through the inlet cavity (Figure 1), at regular intervals, whereas for soaking experiments, the fabricated substrates were soaked in 10 mL of fentanyl solution. SERS measurements for both flow-through and soaking methods were performed on a portable BWTek iRaman Plus (BWS465-5328) system. All of the spectra were recorded within a spectral range of 400−1800 cm^{-1}. The laser excitation used was 532 nm, the acquisition time was 30 s, and the laser power was maintained at 20 mW. For estimation of the limit of detection, a time-dependent study was also performed where the acquisition time was varied up to 60 s. All of the collected spectra were processed using ORIGIN Pro and BEADS for background subtraction, denoising sparsity, and baseline correction.

■ ASSOCIATED CONTENT

Supporting Information

The Supporting Information is available free of charge at https://pubs.acs.org/doi/10.1021/acsomega.3c01519.

Particle size distribution of the functionalized silver nanoparticles and UV−visible spectrum of the synthesized Ag−DE composite. SERS characterization of fentanyl molecules on the fabricated optofluidic device as a function of sample volume (PDF)

■ AUTHOR INFORMATION

Corresponding Author

Alan X. Wang − *School of Electrical Engineering and Computer Science, Oregon State University, Corvallis, Oregon 97331, United States; Department of Electrical and Computer Engineering, Baylor University, Waco, Texas 76798, United States;* orcid.org/0000-0002-0553-498X; Email: alan_wang@baylor.edu

Authors

Subhavna Juneja − *School of Electrical Engineering and Computer Science, Oregon State University, Corvallis, Oregon 97331, United States; Department of Electrical and Computer Engineering, Baylor University, Waco, Texas 76798, United States*

Boxin Zhang − *School of Electrical Engineering and Computer Science, Oregon State University, Corvallis, Oregon 97331, United States*

Complete contact information is available at: https://pubs.acs.org/10.1021/acsomega.3c01519

Author Contributions

§S.J. and B.Z. contributed equally to this work.

Notes

The authors declare no competing financial interest.

https://doi.org/10.1021/acsomega.3c01519
ACS Omega 2023, 8, 17151−17158

■ ACKNOWLEDGMENTS

This work was financially supported by the National Institutes of Health under Grant No. 1R41DA051094, the National Science Foundation under Grant No. 1701329, and the United States Department of Agriculture under Grant No. 2020-33610-31688.

■ REFERENCES

(1) He, R.; Liu, H.; Niu, Y.; Zhang, H.; Genin, G. M.; Xu, F. Flexible miniaturized sensor technologies for long-term physiological monitoring. *npj Flexible Electron.* **2022**, *6*, No. 20.
(2) Shu, J.; Tang, D. Recent Advances in Photoelectrochemical Sensing: From Engineered Photoactive Materials to Sensing Devices and Detection Modes. *Anal. Chem.* **2020**, *92*, 363−377.
(3) Yu, Z.; Gong, H.; Xu, J.; Li, Y.; Zeng, Y.; Liu, X.; Tang, D. Exploiting Photoelectric Activities and Piezoelectric Properties of NaNbO3 Semiconductors for Point-of-Care Immunoassay. *Anal. Chem.* **2022**, *94*, 3418−3426.
(4) Radhakrishnan, S.; Mathew, M.; Rout, C. S. Microfluidic sensors based on two-dimensional materials for chemical and biological assessments. *Mater. Adv.* **2022**, *3*, 1874−1904.
(5) Xing, Y.; Zhao, L.; Cheng, Z.; Lv, C.; Yu, F.; Yu, F. Microfluidics-based sensing of biospecies. *ACS Appl. Bio Mater.* **2021**, *4*, 2160−2191.
(6) Niculescu, A. G.; Chircov, C.; Bîrcă, A. C.; Grumezescu, A. M. Fabrication and applications of microfluidic devices: A review. *Int. J. Mol. Sci.* **2021**, *22*, No. 2011.
(7) Faustino, V.; Catarino, S. O.; Lima, R.; Minas, G. Biomedical microfluidic devices by using low-cost fabrication techniques: A review. *J. Biomech.* **2016**, *49*, 2280−2292.
(8) Terry, S. C.; Jerman, J. H.; Angell, J. B. A gas chromatographic air analyzer fabricated on a silicon wafer. *IEEE Trans. Electron Devices* **1979**, *26*, 1880−1886.
(9) Thangawng, A. L.; Howell, P. B., Jr; Richards, J. J.; Erickson, J. S.; Ligler, F. S. A simple sheath-flow microfluidic device for micro/nanomanufacturing: fabrication of hydrodynamically shaped polymer fibers. *Lab Chip* **2009**, *9*, 3126−3130.
(10) Gale, B. K.; Jafek, A. R.; Lambert, C. J.; Goenner, B. L.; Moghimifam, H.; Nze, U. C.; Kamarapu, S. K. A Review of current methods in microfluidic device fabrication and future commercialization prospects. *Inventions* **2018**, *3*, No. 60.
(11) Luesebrink, H.; Thomas, G.; Stephen, C. J.; John, C. H.; Neil, S. C.; Hélène, R.; Teodor, V. Transition of MEMS technology to nanofabrication. *J. Nanosci. Nanotechnol.* **2005**, *5*, 864−868.
(12) Shopova, S. I.; White, I. M.; Sun, Y.; Zhu, H.; Fan, X.; Frye-Mason, G.; Thompson, A.; Ja, S. J. On-column micro gas chromatography detection with capillary-based optical ring resonators. *Anal. Chem.* **2008**, *80*, 2232−2238.
(13) Kim, T. H.; Hahn, Y. K.; Kim, M. S. Recent Advances of Fluid Manipulation Technologies in Microfluidic Paper-Based Analytical Devices (μPADs) toward Multi-Step Assays. *Micromachines* **2020**, *11*, No. 269.
(14) Yuan, Y.; Panwar, N.; Yap, S. H. K.; Wu, Q.; Zeng, S.; Xu, J.; Tjin, S. C.; Song, J.; Qu, J.; Yong, K.-T. SERS-based ultrasensitive sensing platform: An insight into design and practical applications. *Coord. Chem. Rev.* **2017**, *337*, 1−33.
(15) Parisi, J.; Su, L.; Lei, Y. In situ synthesis of silver nanoparticle decorated vertical nanowalls in a microfluidic device for ultrasensitive in-channel SERS sensing. *Lab Chip* **2013**, *13*, 1501−1508.
(16) Li, Q.-L.; Li, B.-W.; Wang, Y.-Q. Surface-enhanced Raman scattering microfluidic sensor. *RSC Adv.* **2013**, *3*, 13015−13026.
(17) Tong, L.; Righini, M.; Gonzalez, M. U.; Quidant, R.; Käll, M. Optical aggregation of metal nanoparticles in a microfluidic channel for surface-enhanced Raman scattering analysis. *Lab Chip* **2009**, *9*, 193−195.
(18) Yazdi, S. H.; White, I. M. Optofluidic Surface Enhanced Raman Spectroscopy microsystem for sensitive and repeatable on-site detection of chemical contaminants. *Anal. Chem.* **2012**, *84*, 7992−7998.
(19) Sheehan, P. E.; Whitman, L. J. Detection limits for nanoscale biosensors. *Nano Lett.* **2005**, *5*, 803−807.
(20) Han, Y.; Fang, X.; Sun, Z.; Kang, C.; Zha, L.; Zhang, X. Ag nanoparticle-decorated graphene oxide coatings on the inner walls of optofluidic capillaries for real-time trace SERS detection. *ACS Appl. Nano Mater.* **2022**, *5*, 2445−2450.
(21) Fan, X.; White, I. M. Optofluidic microsystems for chemical and biological analysis. *Nat. Photon* **2011**, *5*, 591−597.
(22) Zhou, Q.; Lin, Y.; Zhang, K.; Li, M.; Tang, D. Reduced graphene oxide/BiFeO3 nanohybrids-based signal-on photoelectrochemical sensing system for prostate-specific antigen detection coupling with magnetic microfluidic device. *Biosens. Bioelectron.* **2018**, *101*, 146−152.
(23) Lin, Y.; Zhou, Q.; Li, J.; Shu, J.; Qiu, Z.; Lin, Y.; Tang, D. Magnetic Graphene Nanosheet-Based Microfluidic Device for Homogeneous Real-Time Electronic Monitoring of Pyrophosphatase Activity Using Enzymatic Hydrolysate-Induced Release of Copper Ion. *Anal. Chem.* **2016**, *88*, 1030−1038.
(24) Graham, D. L.; Ferreira, H.; Bernardo, J.; Freitas, P. P.; Cabral, J. M. S. Single magnetic microsphere placement and detection on-chip using current line designs with integrated spin valve sensors: Biotechnological applications. *J. Appl. Phys.* **2002**, *91*, 7786−7788.
(25) Li, H.; Fan, X. Characterization of sensing capability of optofluidic ring resonator biosensors. *Appl. Phys. Lett.* **2010**, *97*, No. 011105.
(26) Escobedo, C.; Brolo, A. G.; Gordon, R.; Sinton, D. Flow-through vs flow-over: Analysis of transport and binding in nanohole array plasmonic biosensors. *Anal. Chem.* **2010**, *82*, 10015−10020.
(27) Kong, X.; Xi, Y.; Le Duff, P.; Chong, X.; Li, E.; Ren, F.; Rorrer, G. L.; Wang, A. X. Detecting explosive molecules from nanoliter solution: A new paradigm of SERS sensing on hydrophilic photonic crystal biosilica. *Biosens. Bioelectron.* **2017**, *88*, 63−70.
(28) Sivashanmugan, K.; Squire, K.; Kraai, J. A.; Tan, A.; Zhao, Y.; Rorrer, G. L.; Wang, A. X. Biological photonic crystal-enhanced plasmonic mesocapsules: approaching single-molecule optofluidic-SERS sensing. *Adv. Opt. Mater.* **2019**, *7*, No. 1900415.
(29) Song, C.; Tan, S. H. A Perspective on the rise of Optofluidics and the future. *Micromachines* **2017**, *8*, No. 152.
(30) Fu, E.; Downs, C. Progress in the development and integration of fluid flow control tools in paper microfluidics. *Lab Chip* **2017**, *17*, 614−628.
(31) Osborn, J. L.; Lutz, B.; Fu, E.; Kauffman, P.; Stevens, D. Y.; Yager, P. Microfluidics without pumps: reinventing the T-sensor and H-filter in paper networks. *Lab Chip* **2010**, *10*, 2659−2665.
(32) Lee, J.; Lee, H. A.; Shin, M.; Juang, L. J.; Kastrup, C. J.; Go, G. M.; Lee, H. Diatom frustule silica exhibits superhydrophilicity and superhemophilicity. *ACS Nano* **2020**, *14*, 4755−4766.
(33) Oliveira, N. M.; Reis, R. L.; Mano, J. F. Superhydrophobic Surfaces Engineered Using Diatomaceous Earth. *ACS Appl. Mater. Interfaces* **2013**, *5*, 4202−4208.
(34) Nguyen, H. H.; Tieu, A. K.; Tran, B. H.; Wan, S.; Zhu, H.; Pham, S. T. Porosity-induced mechanically robust superhydrophobicity by the sintering and silanization of hydrophilic porous diatomaceous earth. *J. Colloid Interface Sci.* **2021**, *589*, 242−251.
(35) Roychoudhury, P.; Bose, R.; Dąbek, P.; Witkowski, A. Photonic nano-/microstructured diatom based biosilica in metal modification and removal—a review. *Materials* **2022**, *15*, No. 6597.
(36) Wang, Z.; Gong, D.; Cai, J. Diatom frustule array for flow-through enhancement of fluorescent signal in a microfluidic chip. *Micromachines* **2021**, *12*, No. 1017.
(37) Fang, Y.; Chen, V. W.; Cai, Y.; Berrigan, J. D.; Marder, S. R.; Perry, J. W.; Sandhage, K. H. Biologically Enabled Syntheses of Freestanding Metallic Structures Possessing Subwavelength Pore Arrays for Extraordinary (Surface Plasmon-Mediated) Infrared Transmission. *Adv. Funct. Mater.* **2012**, *22*, 2550−2559.

https://doi.org/10.1021/acsomega.3c01519
ACS Omega 2023, 8, 17151−17158

(38) Shen, Z.; Fan, Q.; Yu, Q.; Wang, R.; Wang, H.; Kong, X. Facile detection of carbendazim in food using TLC-SERS on diatomite thin layer chromatography. *Spectrochim. Acta, A* **2021**, *247*, No. 119037.
(39) Chen, J.; Qin, G.; Chen, Q.; Yu, J.; Li, S.; Cao, F.; Yang, B.; Ren, Y. A synergistic combination of diatomaceous earth with Au nanoparticles as a periodically ordered, button-like substrate for SERS analysis of the chemical composition of eccrine sweat in latent fingerprints. *J. Mater. Chem. C* **2015**, *3*, 4933−4944.
(40) Jiang, X.; Zeng, Q.; Yu, A. A self-seeding coreduction method for shape control of silver nanoplates. *Nanotechnology* **2006**, *17*, 4929−4935.
(41) Juneja, S.; Bhattacharya, J. Biosynthetically grown dendritic silver nanostructures for visible Surface Enhanced Resonance Raman Spectroscopy (v-SERRS). *New J. Chem.* **2020**, *44*, 16163−16173.
(42) Leonard, J.; Haddad, A.; Green, O.; Birke, R. L.; Kubic, T.; Kocak, A.; Lombardi, J. R. SERS, Raman, and DFT analyses of fentanyl and carfentanil: toward detection of trace samples. *J. Raman Specteosc.* **2017**, *48*, 1323−1329.
(43) Qin, Y.; Yin, S.; Chen, M.; Yao, W.; He, Y. Surface-enhanced Raman spectroscopy for detection of fentanyl and its analogs by using Ag-Au nanoparticles. *Spectrochim. Acta, A* **2023**, *285*, No. 121923.
(44) Sivaprakasam, V.; Hart, M. B. Surface-Enhanced Raman Spectroscopy for Environmental Monitoring of Aerosols. *ACS Omega* **2021**, *6*, 10150−10159.
(45) Zhang, M.; Pan, L.; Xu, X.; Fu, G.; Zhang, L.; Sun, P.; Yan, X.; Liu, F.; Wang, C.; Liu, X.; Lu, G. Gold-trisoctahedra-coated capillary-based SERS platform for microsampling and sensitive detection of trace fentanyl. *Anal. Chem.* **2022**, *94*, 4850−4858.
(46) Mirsafavi, R.; Moskovits, M.; Meinhart, C. Detection and classification of fentanyl and its precursors by surface-enhanced Raman spectroscopy. *Analyst* **2020**, *145*, 3440−3446.
(47) Qin, Y.; Wang, B.; Wu, Y.; Wang, J.; Zong, X.; Yao, W. Seed-mediated preparation of Ag@Au nanoparticles for highly sensitive surface-enhanced Raman detection of fentanyl. *Crystals* **2021**, *11*, 769−779.
(48) Wilson, N. G.; Raveendran, J.; Docoslis, A. Portable identification of fentanyl analogues in drugs using surface-enhanced Raman scattering. *Sens. Actuators, B* **2021**, *330*, 129303−129311.
(49) Haddad, A.; Comanescu, M. A.; Green, O.; Kubic, T. A.; Lombardi, J. R. Detection and quantitation of trace fentanyl in heroin by surface-enhanced Raman spectroscopy. *Anal. Chem.* **2018**, *90*, 12678−12685.
(50) Shende, C.; Brouillette, C.; Farquharson, S. Detection of codeine and fentanyl in saliva, blood plasma and whole blood in 5-minutes using a SERS flow-separation strip. *Analyst* **2019**, *144*, 5449−5454.
(51) Shende, C.; Farquharson, A.; Brouillette, C.; Smith, W.; Farquharson, S. Quantitative measurements of codeine and fentanyl on a surface-enhanced Raman-active pad. *Molecules* **2019**, *24*, 2578−2586.
(52) Zhang, B.; Hou, X.; Zhen, C.; Wang, A. X. Sub-part-per-billion level sensing of fentanyl residues from wastewater using portable Surface-enhanced Raman scattering sensing. *Biosensors* **2021**, *11*, No. 370.
(53) Sivashanmugan, K.; Squire, K.; Tan, A.; Zhao, Y.; Joseph Abraham Kraai, J. A.; Rorrer, G. L.; Wang, A. X. Trace detection of tetrahydrocannabinol in body fluid via surface enhanced Raman scattering and principal component analysis. *ACS Sens.* **2019**, *4*, 1109−1117.
(54) Kong, X.; Xi, Y.; LeDuff, P.; Li, E.; Liu, Y.; Cheng, L.-J.; Rorrer, G. L.; Tan, H.; Wang, A. L. Optofluidic sensing from inkjet-printed droplets: the enormous enhancement by evaporation induced spontaneous flow on photonic crystal biosilica. *Nanoscale* **2016**, *8*, 17285−17294.

https://doi.org/10.1021/acsomega.3c01519
ACS Omega 2023, 8, 17151−17158